Charge extraction by a linearly increasing voltage of photo-generated carriers: The influence of two mobile carrier types, bimolecular recombination, and series resistance

Oskar J. Sandberg[1,2] and Mathias Nyman[2]

[1]Department of Physics, Swansea University, Singleton Park, Swansea SA2 8PP Wales, United Kingdom
[2]Physics, Center for Functional Materials and Faculty of Science and Technology, Åbo Akademi University, Porthaninkatu 3, 20500 Turku, Finland

E-mail: osandber@abo.fi, mathnyma@abo.fi

Abstract

The charge extraction by a linearly increasing voltage (CELIV) technique is a well-known and commonly used method to characterize charge transport in low-mobility materials. In the original CELIV theory it is assumed that one type of charge carrier is mobile and the other fixed and that recombination during the extraction pulse is negligible. However, this is in general not the case, especially in photo-CELIV where both electrons and holes are generated by light excitation. Moreover, RC effects induced by the series or load resistance of the external circuit are typically assumed to be negligible. In this work, we use drift-diffusion modelling and analytical derivations to show that the standard equations used for calculating the mobility in the moderate conductivity regimes generally leads to errors in the mobility determination in the case when i) two carrier types of similar mobility, ii) recombination, iii) an electric-field-dependent mobility, and iv) RC effects are present in the device. The effect of the external series resistance on the mobility determination becomes of particular importance in devices with relatively large mobilities and/or high carrier concentrations, where the original CELIV theory might give rise to an underestimation of the mobility by several orders of magnitude.

1. Introduction

Organic semiconductors are an interesting class of materials due to their solution processability and potential for future low-cost electronic components. Organic semiconductors typically have low charge carrier mobilities due to a broad density of states caused by disorder, which limits their performance. In order to drive the field forward it is important to develop better performing materials and for this, it is vital to have reliable characterization techniques.

The Charge Extraction by a Linearly Increasing Voltage (CELIV) technique, first demonstrated by Juška *et al* on microcrystalline silicon, has become one of the most commonly used methods to characterize charge transport in low- to moderate-mobility materials.[1,2] The advantage of CELIV is that it can be used directly on operating devices, such as organic solar cells and diodes, to simultaneously determine the charge carrier concentration and mobility. The technique has later been extended to the case when charges are generated via photo-excitation in thin-film active layers (photo-CELIV and OTRACE),[3-5] and via dark injection into metal-insulator-semiconductor structures[6-8] (MIS-CELIV).

In a photo-CELIV (photo-induced charge extraction by linearly increasing voltage) measurement, charge carriers are photo-generated in a (thin) semiconductor layer. The photo-induced carriers are subsequently extracted by applying a linear voltage pulse (in reverse bias) and the corresponding extraction current transient, given by

$$j(t) = j_0 + \Delta j(t) \qquad (1)$$

is recorded. In Eq. (1), $\Delta j(t)$ is the average conduction current of mobile charge carriers within the active layer and $j_0 = CA$ is the average displacement current, where C is the geometric capacitance of the active layer and A is the voltage ramp up rate. From the time of the extraction current maximum t_{max}, the mobility μ of the carriers can be calculated.[1,9] To avoid charge extraction prior

to the ramp up pulse, a compensating offset voltage is typically used. The premature extraction can further be minimized by keeping the device at open-circuit conditions prior to the ramp up pulse, this extension of the photo-CELIV technique is referred to as OTRACE (open circuit corrected transient CELIV).[5] In this work, the basic theory behind the mobility determination in photo-CELIV is revisited by means of numerical simulations and analytical derivations.

2. Theoretical background

Starting from a uniform generation of the photo-induced carriers, assuming open-circuit conditions (flat-band), the average conduction current of extracted charge carriers, induced by applying the ramp up voltage pulse at $t = 0$, can be expressed as

$$\Delta j(t) = \frac{en}{d}\left[\int_{l_n(t)}^{d} \mu_n F(x,t)\, dx + \int_{0}^{d-l_p(t)} \mu_p F(x,t)\, dx\right] \qquad (2)$$

taking diffusion to be negligible. Here, d is the thickness of the active semiconductor layer assumed to be undoped, n is the photo-induced carrier density, and $F(x,t)$ is the electric field, while $\mu_{n(p)}$ and $l_{n(p)}(t)$ is the mobility and extraction depth for electrons (holes), respectively. The electrons (holes) are extracted at $x = d$ ($x = 0$) during the linear voltage pulse. In the following, electrons are assumed to be the faster carrier type, *i.e.* $\mu_n > \mu_p$.

In accordance with the basic CELIV theory originally presented by Juška *et al* and later refined by Lorrmann *et al*,[1,9] the following additional assumptions are made:

i) The slower carrier type is assumed to be immobile, in this case corresponding to $\mu_p = l_p = 0$, whereas $\mu_n = \mu$ and $l_n = l(t)$.

ii) The recombination between electrons and holes during the extraction pulse, or within the time interval $0 \leq t \leq t_{max}$, is negligible.

iii) The mobility is assumed to be constant and independent of the electric field within the active layer.

iv) Resistive voltage losses are neglected, corresponding to a series resistance of the external circuit given by $R = 0$.

Under these circumstances, Eq. (2) reduces to[1,9]

$$\Delta j(t) = en\frac{dl(t)}{dt}\left[1 - \frac{l(t)}{d}\right] \tag{3}$$

with

$$\frac{dl(t)}{dt} = \mu F(d,t) = \frac{\mu}{d}\left[At - \frac{en}{2\varepsilon\varepsilon_0}l^2(t)\right] \tag{4}$$

where $F(d,t)$ is the electric field in the region $l(t) < x < d$ and $l(0) = 0$. The second term on the right-hand side of Eq. (4) represents the reduction (redistribution) of the extracting electric field due to the (fixed) space charge of the immobile carriers. In the low-conductivity regime, corresponding to $\Delta j \ll j_0$, this space charge term is negligible; in this limit $\mu = 2d^2/3At_{max}^2$.[1] For moderate conductivities $\Delta j_{max} \sim j_0$, on the other hand, the (faster) mobility is obtained from[9]

$$\mu = K_\sigma^2 \frac{2d^2}{3At_{max}^2} \tag{5}$$

$$K_\sigma = \frac{\sqrt{3}}{2}\left[\frac{1}{6.2\left(1+0.002\frac{\Delta j_{max}}{j_0}\right)} + \frac{1}{1+0.12\frac{\Delta j_{max}}{j_0}}\right] \tag{6}$$

as suggested by Lorrmann *et al*, where $\Delta j_{max} \equiv \Delta j(t_{max})$.

3. Results and discussion

In the following, the effects of two mobile charge carriers, bimolecular recombination during the extraction process, electric-field-dependent mobilities, and external series resistance on the mobility determination using photo-CELIV (or OTRACE) are separately clarified. In this study we use a numerical model that solves the charge continuity and drift-diffusion equations for electrons

and holes, in conjunction with the Poisson equation which accounts for the space charge effects in the active layer.[10,11] The carriers are initially assumed to have equal and uniform densities throughout the layer. At $t \geq 0$, these carriers are subsequently extracted by the ramp up voltage pulse, leading to a current of the form in Eq. (1), from which the t_{max} is determined.

3.1 The case with two mobile carriers

In the original CELIV theory, as presented above, the slower charge carrier is assumed to be fixed. In general, however, both carriers are mobile; in this case, the situation becomes more complicated. Nonetheless, analytical solutions can be obtained in the limit of low carrier concentrations when space charge effects are negligible ($\Delta j_{max}/j_0 \rightarrow 0$). Under these conditions, the electric field approximates as $F \approx At/d$. Then, after noting that $dl_{n(p)}/dt = \mu_{n(p)}F$, and subsequently $l_{n(p)}(t) = \mu_{n(p)}At^2/2d^2$ for $0 \leq l_{n(p)}(t) \leq d$, Eq. (2) can be evaluated. The associated (first peak) t_{max} in the limit $\Delta j_{max}/j_0 \rightarrow 0$ (low-conductivity regime) is thus related to the mobilities via

$$t_{max,0} = d\sqrt{\frac{2}{3\mu_{\text{eff}}A}} \tag{7}$$

where μ_{eff} is the effective (apparent) mobility given by

$$\mu_{\text{eff}} \equiv \frac{\mu_n^2+\mu_p^2}{\mu_n+\mu_p} \tag{8}$$

The effective mobility μ_{eff} depends on both of the carrier mobilities. As expected, however, t_{max} (Eq. (7)) is strongly dominated by the carrier with the larger mobility in this limit, with μ_{eff} deviating from the faster mobility by only 17% at most.

At $\Delta j_{max} \sim j_0$, however, space charge effects generally become important. To clarify these issues, we turn to numerical drift-diffusion simulations to investigate the effect of two carrier types with

different but comparable mobilities. The parameters used in the simulations are: $\mu_n = 10^{-4}$ cm^{2}V^{-1}s^{-1} and $d = 200$ nm. Moreover, unless otherwise stated, we assume $n = 6 \times 10^{15}$ cm^{-3} and $A = 10^5$ Vs^{-1}, with the duration of the voltage pulse given by $t_{pulse} = 20$ µs.

Simulated CELIV current transients at different mobility ratios μ_p/μ_n for the slower carrier type (holes) are shown in Fig. 1(a). From Fig. 1(a) it can be seen that Eq. (5) increasingly underestimates the mobility of the faster carriers (electrons) when the hole mobility becomes comparable to the electron mobility. This is further demonstrated in Fig. 1(b), where the corresponding mobilities, as extracted from the simulated CELIV current transients using Eq. (5), are shown for different $\Delta j_{max}/j_0$ obtained by varying the density of photo-induced carriers (varying light intensity). At $\Delta j_{max} \sim 10 j_0$, the mobility is underestimated by a factor-of-three if the mobilities are balanced.

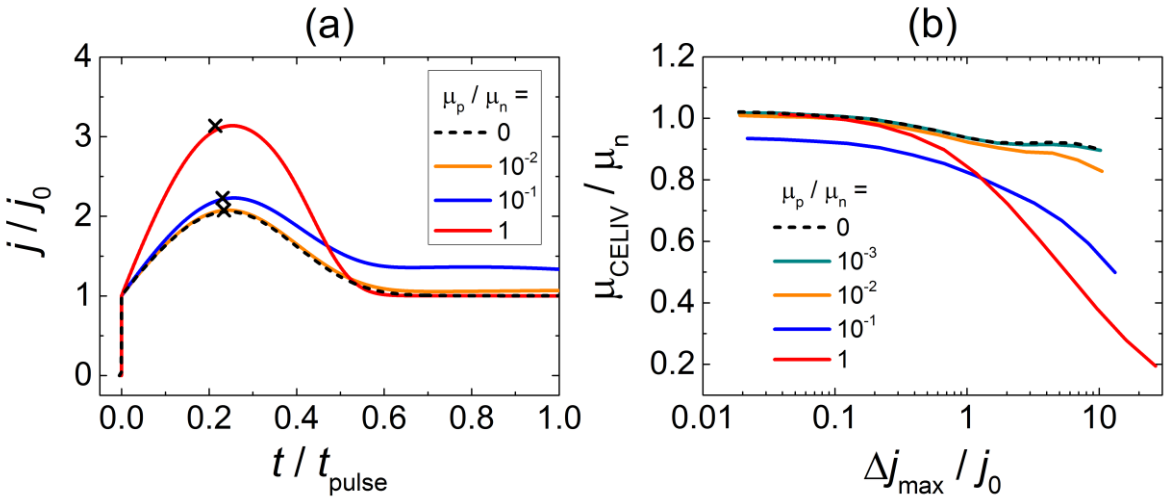

Fig. 1. (a) Simulated CELIV current transients at different mobilities of the slower carrier type. The electron mobility is set to $\mu_n = 10^{-4}$ cm^{2}V^{-1}s^{-1} and the initial carrier densities are 6×10^{15} cm^{-3}. The predicted position of t_{max}, as per Eq. (5), is indicated by the crosses. (b) The corresponding normalized mobilities $\mu_{\mathrm{CELIV}}/\mu_n$, as extracted from the simulated CELIV current transients using Eq. (5), are shown as a function of $\Delta j_{max}/j_0$ at different mobilities. The current extraction maximum Δj_{max} is varied by changing the initial concentrations ($n = p$) of photo-induced carriers (from 10^{14} to 10^{17} cm^{-3}).

Fig. 2 shows the corresponding t_{max} as extracted from the simulated extraction current transients, normalized to $t_{max,0}$ (Eq. (7)), at different voltage ramp up rates (A). The mobility extracted by Eq. (5) coincides well with the effective mobility μ_{eff} at small $\Delta j_{max}/j_0$. Similarly, when the ratio between the mobilities is large, the slower carrier is effectively immobile and Eq. (5) provides a good approximation for the mobility determination of the faster carrier. The small deviations seen at large $\Delta j_{max}/j_0$ are attributed to diffusion. When the mobilities are comparable, on the other hand, the situation is distinctly different. Under these conditions, space charge effects become less pronounced, as charge carriers within the space charge regions do not remain fixed but redistribute in accordance with the electric field. This is manifested as an apparent A dependence of the extracted mobility, which might be misinterpreted as an electric-field dependence of the mobility. Based on the simulations in Fig. 2, t_{max} can be expressed as

$$t_{max} = K\sqrt{\frac{2d^2}{3A\mu_{\text{eff}}}} \tag{9}$$

where K is a numerical factor which takes a value between $K = 1$ (low-conductivity limit) and $K = K_\sigma$ (moderate-conductivity correction, Eq. (6)). Hence, the correct effective mobility is somewhere between the low-conductivity limit and the moderate-conductivity approximation in case of a general μ_p/μ_n. This uncertainty is larger for larger $\Delta j_{max}/j_0$. In the limit of small $\Delta j_{max}/j_0$ and large A, in turn, the error in the mobility determination is reduced. It should, however, be stressed that the extracted photo-CELIV mobility, given by μ_{eff}, is dominated by the faster carriers. This is one of the main disadvantages with the photo-CELIV and OTRACE techniques; it is challenging to determine charge carrier mobilities selectively, especially in thin films.

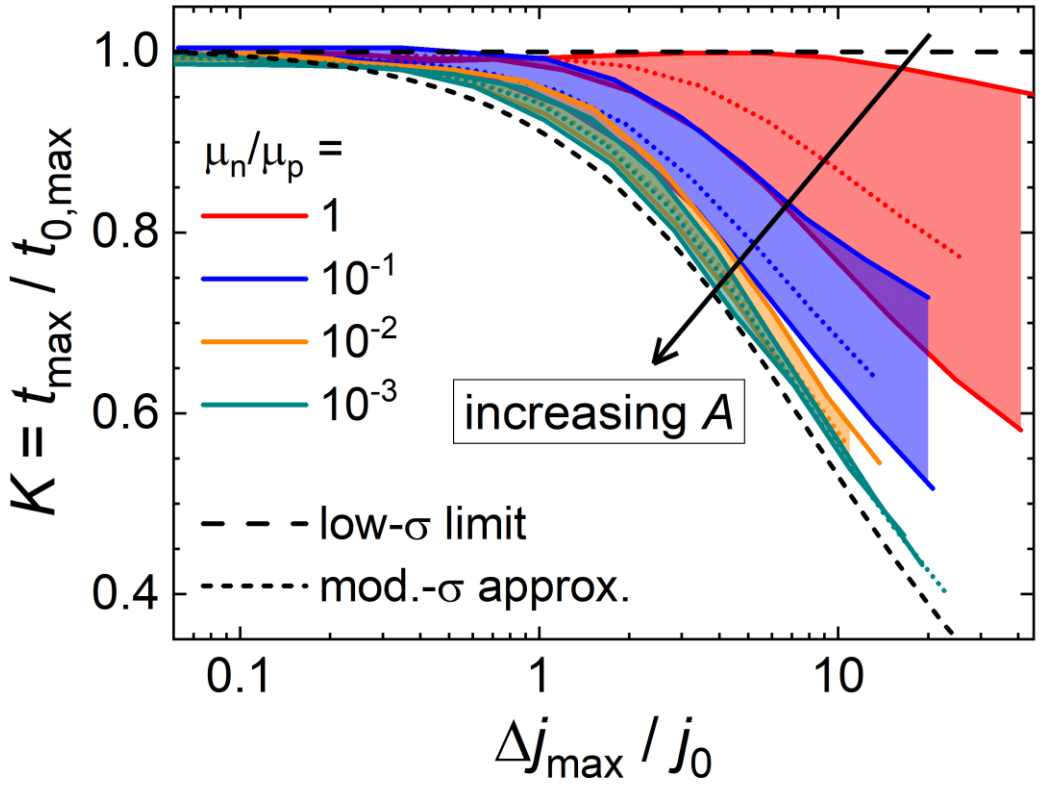

Fig. 2. Simulated $K = t_{max}/t_{0,max}$ as a function of $\Delta j_{max}/j_0$ for the different mobilities at different voltage rise speeds A. Here, $t_{0,max} = d\sqrt{2/3\mu_{\text{eff}}A}$ corresponds to the theoretical t_{max} in the low-conductivity limit (Eq. (6)), with the effective mobility $\mu_{\text{eff}} = (\mu_n^2 + \mu_p^2)/(\mu_n + \mu_p)$. The upper and lower solid lines (which confine the shaded areas) for the different μ_n/μ_p correspond to $A = 10^4$ V/s and $A = 10^6$ V/s, respectively, whereas the (colored) dotted lines indicate the case with $A = 10^5$ V/s from Fig. 1. The initial carrier concentrations are varied from 10^{14} to 10^{17} cm^{-3}. The low and moderate conductivity (σ) approximations, respectively, correspond to $K = 1$ (see Eq. (6)) and $K = K_\sigma$ (Eq. (5)).

It has recently been proposed that the electron and hole mobilities can be separated in photo-CELIV by inserting a charge-blocking layer at one of the collecting contacts.[12,13] In these "charge-selective photo-CELIV" studies, the purpose of the blocking layer is to prevent the extraction of one type of photo-induced carrier (hole or electron, depending on the position of this layer) to the external

circuit during the measurement, resulting in the other carrier type supposedly dominating the CELIV current transient. The basic problem with this approach is that both carrier types are still mobile within the semiconductor layer during the extraction process (photo-generated electrons and holes drift toward the cathode and anode, respectively), and thus contribute to the local conduction current. The fact that carriers moving within (a specific region of) the active layer induce a current flow (across the entire device) is of course the theoretical foundation behind all current transient methods, including time-of-flight, dark injection, conventional CELIV (incl. photo-CELIV and OTRACE), and MIS-CELIV.[1,7-9,14-17]

In Fig. 3(a), photo-CELIV current transients, simulated for the case when $\mu_p/\mu_n \to 0$, are shown for a device with and without an electron-blocking layer at the electron-colleting cathode contact (at $x = d$). The blocking layer is assumed perfectly blocking.[18] As evident from Fig. 3(a), the shape and magnitude of the extraction current transients (of electrons) are almost identical, regardless of the blocking layer. In Fig. 3(b), the corresponding average electron concentrations (inside the active layer), as a function of time, are simulated. It can be seen that although no electrons are extracted to the external circuit (since the average electron density inside the active layer is unchanged), a (non-suppressed) electron current transient is still obtained. This current arises when electrons, initially uniformly distributed throughout the active layer, move towards the blocking contact (and accumulate there without being extracted, see inset of Fig. 3(b)). The case when both electrons and holes are mobile and have comparable mobilities, $\mu_p = 10^{-1} \times \mu_n$, is demonstrated in Fig. 3(c). Again, t_{max} is dominated by the faster carrier (in our case electrons), regardless of whether the electron-collecting contact is blocking or not. Hence, the presence of a charge-selective blocking layer alone is not enough to suppress the transient current of the carriers that cannot be extracted to the outer circuit.

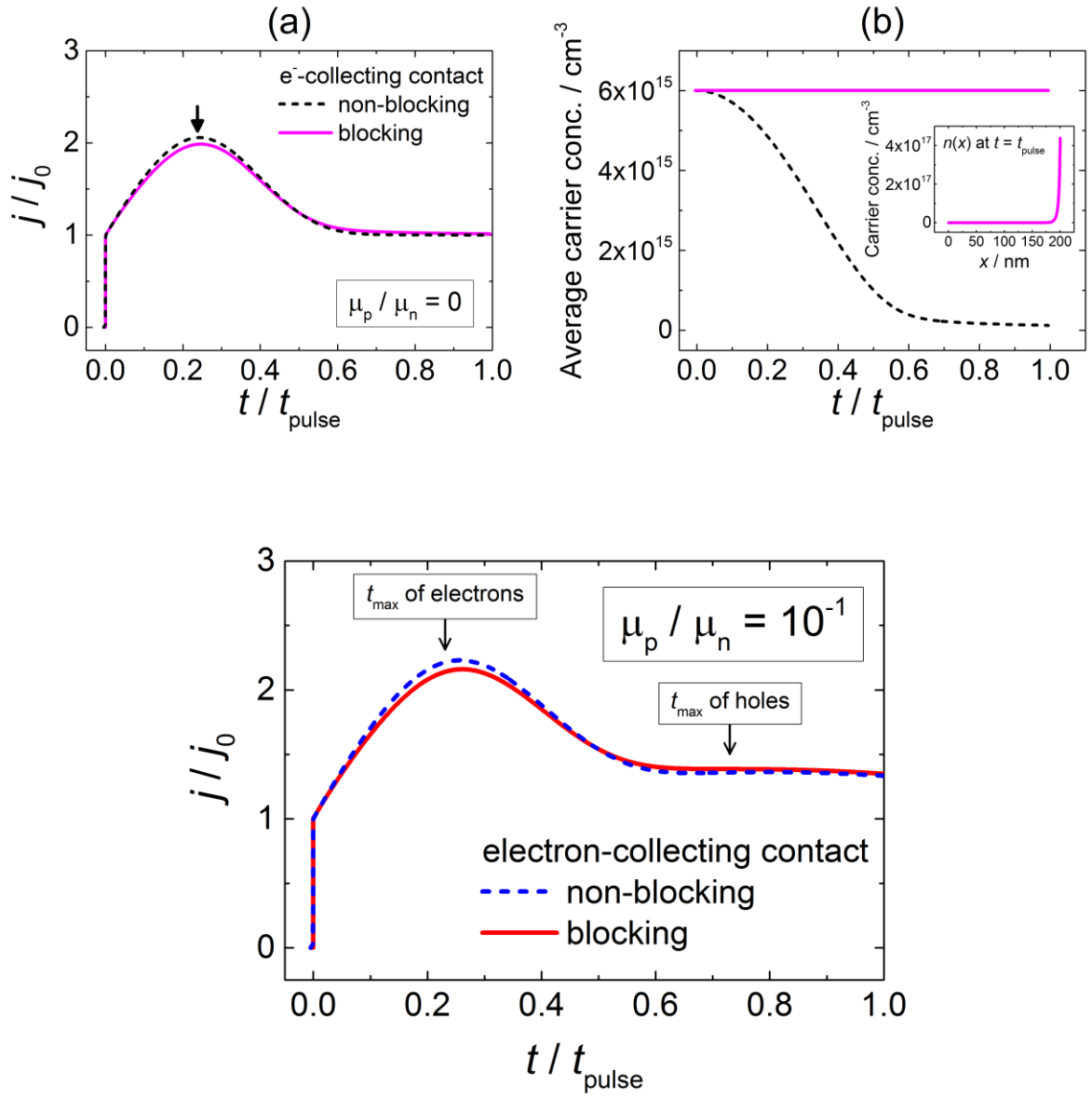

Fig. 3. (a) Simulated CELIV current transients for the case with and without a blocking layer at the carrier-collecting contact. The electron mobility is set to $\mu = 10^{-4}$ cm^{2}V^{-1}s^{-1}, whereas the holes are immobile; the initial carrier densities are 6×10^{15} cm^{-3}, $A = 10^5$ Vs^{-1}, $t_{pulse} = 20$ µs, and $d = 200$ nm. In (b) the corresponding average electron concentration within the active layer as a function of extraction time is shown. The inset shows the local electron density at the end of the pulse for the case with blocking contacts. In (c) the corresponding photo-CELIV current transients for the case when $\mu_n = 10\mu_p$. The position of t_{max}, as expected by Eq. (5), for electrons and holes are indicated by the arrows.

3.2 The impact of bimolecular recombination

In general, the mobility determination is also influenced by recombination.[19-21] Recombination reduces the carrier density within the active layer during the extraction process. For a bimolecular recombination rate of the form $dn/dt = -\beta n^2$, the carrier density depends on the time in accordance with

$$n(t) = \frac{n(0)}{[1+\beta n(0)t]} \tag{10}$$

where β is the recombination coefficient and $n(0)$ is the carrier density at $t = 0$.

An analytical approximation for $\Delta j(t)$ in the low-conductivity limit (when the second term in Eq. (4) is negligible), that accounts for the effect of bimolecular recombination, can be obtained by substituting Eq. (10) into Eq. (3). The associated t_{max} is then given by

$$\frac{t_{max}(\beta)}{t_{max}(0)} = \sqrt{1 - \frac{\beta \Delta j_{max}}{\beta_L j_0}} \tag{11}$$

where $\beta_L = q\mu/\varepsilon\varepsilon_0$ and $t_{max}(0)$ is the corresponding time of maximum in the absence of recombination ($\beta \to 0$). The effect of bimolecular recombination is to reduce t_{max}, which might lead to a severe overestimation of the mobility in photo-CELIV if the recombination is not taken into account.

Bange *et al* investigated the effect of bimolecular recombination on t_{max} by numerical simulations.[19] Fig. 4(a) shows the t_{max} vs. $\Delta j_{max}/j_0$ simulated by Bange *et al* (see Ref. [19]), as indicated by the symbols, at different β. Comparing the numerical simulations with the analytical approximation (Eq. (11)) obtained in our work, an excellent agreement is indeed found at small $\Delta j_{max}/j_0$. In fact, a rather good overall agreement is also found at moderate $\Delta j_{max}/j_0$. Hence, for the general case we may approximate

$$\mu = K^2 \frac{2d^2}{3At_{max}^2}\left[1 - \frac{\beta \Delta j_{max}}{\beta_L j_0}\right] \tag{12}$$

The effect of recombination on the mobility determination can thus be taken into account by introducing an additional correction factor $[1 - \beta \Delta j_{max}/\beta_L j_0]$. It should be noted that in the limit of large $\Delta j_{max}/j_0$ (large light intensities) the transient current saturates to $\Delta j_{max}/j_0 \rightarrow \beta_L/\beta$.[21]

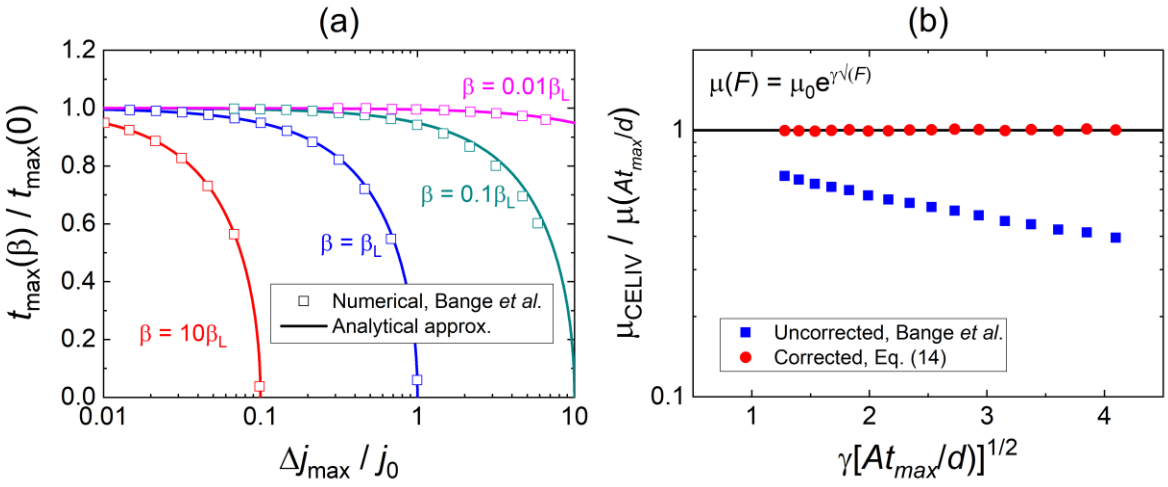

Fig. 4. In (a) the influence of bimolecular recombination on t_{max} relative to the case without recombination, is shown as a function of $\Delta j_{max}/j_0$. The analytical approximation Eq. (11), obtained in this work, is depicted by the solid lines. For comparison, the numerical simulations by Bange *et al.* (Ref. [19]) are included and indicated by the symbols. In (b) the impact of a Poole-Frenkel-type electric-field-dependent mobility (Eq. (13)) on extracted CELIV mobility is shown. The blue squares and red circles correspond to numerical data points that are uncorrected and corrected (as per Eq. (14)) for the electric-field dependence, respectively. The numerical data was taken from Bange *et al.* (Ref. [19]).

3.3 Electric-field-dependent charge carrier mobility

In most organic materials, the mobility also depends on the electric field inside the active layer. In many cases a Poole-Frenkel-type electric-field dependence of the mobility is observed, taking the form[22-24]

$$\mu(F) = \mu_0 \exp\left(\gamma\sqrt{F}\right) \qquad (13)$$

where μ_0 is the zero-field mobility and γ is the Poole-Frenkel coefficient. Under these conditions, the mobility will increase with time during the extraction pulse, distorting the mobility determination. Taking the mobility extracted with Eq. (5) to correspond to the mobility at $t = t_{max}$ generally underestimates the actual mobility at $t = t_{max}$.[19]

The impact of Eq. (13) can be evaluated analytically under conditions when space charge effects (second term on the right-hand side of Eq. (4)) are negligible; by inserting Eq. (13) into Eq. (4) and integrating, an expression for $l(t)$ can in this case be obtained.[19,25] In the limit of a weak electric-field dependence, $\gamma\sqrt{At_{max}/d} \ll 1$, the low-conductivity approximation $\mu = 2d^2/3At_{max}^2$ is obtained, as expected. Here, At_{max}/d corresponds to the electric field inside the active layer at $t = t_{max}$. Conversely, in the limit of strong electric-field dependences $\gamma\sqrt{At_{max}/d} \gg 1$, we obtain $\mu\left(F = \sqrt{At_{max}/d}\right) = (d^2/4At_{max}^2) \times \gamma\sqrt{At_{max}/d}$. In this limit, the low-conductivity approximation underestimates the mobility (at $t = t_{max}$) by a factor of $0.375\gamma\sqrt{At_{max}/d}$.

In the intermediate regime, the mobility can be related to the t_{max}, to a good approximation, via the following expression

$$\mu = \mu_0 \exp\left(\gamma\sqrt{\frac{At_{max}}{d}}\right) = K^2 \frac{2d^2}{3At_{max}^2}\left[1 + \frac{3}{8}\gamma\sqrt{\frac{At_{max}}{d}}\right] \qquad (14)$$

which correctly approaches the above limiting cases in the limits of weak and strong electric-field dependences. In Fig. 4(b), the analytical approximation Eq. (14) is compared to numerical simulations by Bange *et al* (Ref. [19]); the agreement is excellent. We note that for typical values of $\gamma \sim 10^{-3}\sqrt{\text{cm/V}}$ (depending on the temperature) and $\sqrt{At_{max}/d} = 100\sqrt{\text{V/cm}}$,[26] the correction due to the electric-field dependence will be small.

3.4 The effect of the external series resistance

In the derivation of the original CELIV theory, resistive voltage losses due to the series resistance of the external circuit was neglected. The series resistance reduces the applied transient voltage across the active layer as $U(t) = U_0(t) - jR$, where $R = R_S \times S$ with R_S being the total external series resistance (in Ω), S is the device area, and $U_0(t)$ is the external applied voltage.[27] Subsequently, the current equation (Eq. (1)) is modified as

$$j(t) = \Delta j(t) + j_0 - RC\frac{\partial j(t)}{\partial t} \qquad (15)$$

where $\Delta j(t)$ is the average conduction current over the active layer and $j_0 = CA$ with $A = \partial U_0/\partial t$, as before. Here, the geometric capacitance is given by $C = \varepsilon\varepsilon_0/d$. In accordance with Eq. (15), the transient current density is then given by

$$j(t) = \int_0^t \frac{\Delta j(t')}{RC}\exp\left(\frac{t'-t}{RC}\right)dt' + j_0\left[1 - \exp\left(-\frac{t}{RC}\right)\right] \qquad (16)$$

with $\Delta j(t')$ given by Eq. (3). The RC time constant may be approximated from the slope of the transient current rise at $t = 0$ since $j(t) \approx j_0[t/RC]$ at very small times.[27]

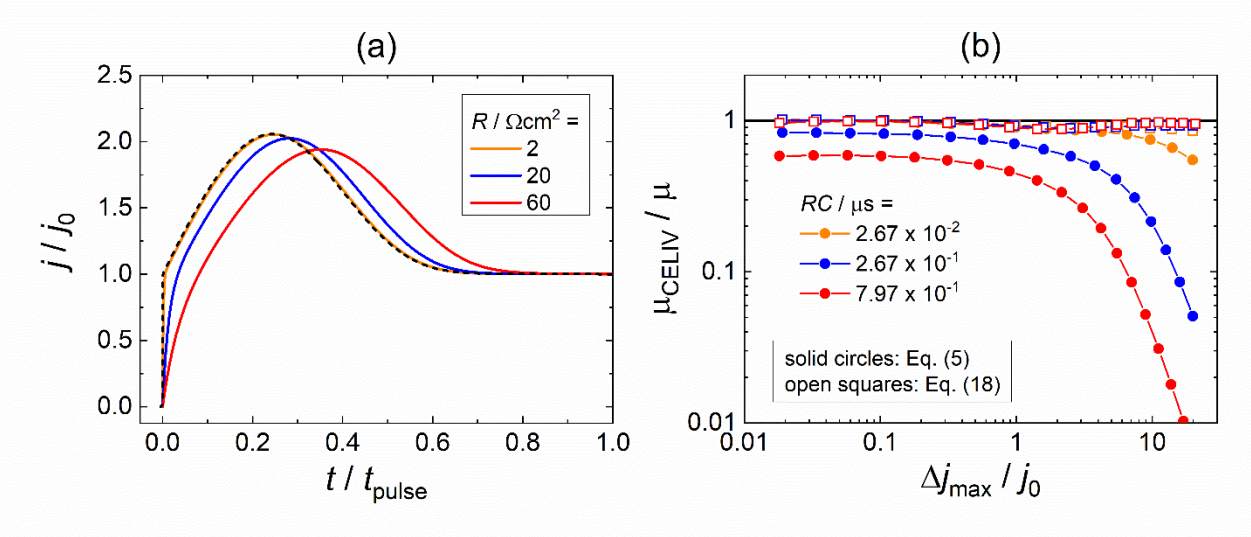

Fig. 5. (a) Simulated CELIV current transients for different RC time constants. For $S = 0.10$ cm^2, the orange, blue and red line correspond to $R_S = 20$ Ω, $R_S = 200$ Ω, and $R_S = 600$ Ω, respectively. The case without series resistance

is indicated by the black dashed line and is identical to the case $\mu_p = 0$ in Fig. 1(a) (and $\mu_n = \mu$). (b) The corresponding mobilities μ_{CELIV}/μ vs. $\Delta j_{max}/j_0$, as extracted using Eq. (5), are indicated by the lines with the solid circles. Here, $\Delta j_{max}/j_0$ is varied by varying the carrier density (light intensity). The lines with open squares depict the mobilities obtained by Eq. (18), which accounts for RC effects.

In the following, we extend the basic CELIV theory, presented in Section 2, to the case with a finite RC time constant. To account for the series resistance in Eq. (4), the term At needs to be replaced by $At - Rj(t)$. Then, after making use of Eq. (15) and Eq. (3), Eq. (4) is modified as

$$\left[1 + \frac{RC}{\tau_\sigma}\right]\frac{\partial l(t)}{\partial t} + RC\,\frac{\partial^2 l(t)}{\partial t^2} = \frac{\mu}{d}\left[At - \frac{en}{2\varepsilon\varepsilon_0}\,l^2(t)\right] \qquad (17)$$

where $\tau_\sigma = \varepsilon\varepsilon_0/\sigma$ is the dielectric relaxation constant, with $\sigma = qn\mu$ being the (photo-induced) conductivity of the active layer. Note that $RC/\tau_\sigma = R/R_{bulk}$, where $R_{bulk} = d/en\mu$ is the (initial) photo-induced resistance (in units of $\Omega\mathrm{m}^2$) of the active layer. At low conductivities, Eq. (17) can be solved analytically, allowing for an approximation for t_{max} to be obtained.[28] Based on this analysis, we find

$$\mu = \frac{2K_\sigma^2 d^2}{3At_{max}^2}\left[1 + \frac{RC}{\tau_\sigma}\right]\left[1 - B\,\frac{RC}{t_{max}} + \left(B + \frac{4/3}{\left[1+\frac{RC}{\tau_\sigma}\right]^2}\right)\left(\frac{RC}{t_{max}}\right)^2\right]^{-1} \qquad (18)$$

for $t_{max} > 4RC$, where $B \equiv (4\tau_\sigma + 2RC)/(\tau_\sigma + RC)$ and we included the additional factor K_σ to correct for moderate conductivities. Note that in the limit $RC \to 0$, Eq. (18) reduces to Eq. (5) as expected.

In Fig. 5(a), CELIV current transients are simulated at different RC times. As expected, the effect of increasing the RC time constant is to delay the current maximum, leading to an underestimation of the mobility. The corresponding CELIV mobilities, as extracted from the simulated extraction current transients using Eq. (5) (solid symbols), are depicted in Fig. 5(b), showing an increasing error with increasing RC time constant and carrier density ($\Delta j_{max}/j_0$). The RC-induced error is,

however, significantly reduced when using Eq. (18) instead, as indicated by the open symbols in Fig. 5(b). At small $\Delta j_{max}/j_0$ (large τ_σ), the deviation obtained by Eq. (5) is a consequence of t_{max} becoming comparable to the RC time constant. In accordance with Eq. (18), this effect can be corrected for by effectively replacing t_{max}^2 in Eq. (5) with the quantity $[(t_{max} - 2RC)^2 + 4(RC)^2/3]$.

At larger $\Delta j_{max}/j_0$, the effect of the series resistance increases drastically as the interplay between the RC time constant and τ_σ becomes important. When the RC time and/or the carrier density is large enough for $\tau_\sigma < RC$, the effective bulk resistance of the active layer becomes smaller than the series resistance of the external circuit. Under these conditions, Eq. (18) may be simplified as

$$\mu \approx K_\sigma^2 \frac{2d^2}{3At_{max}^2}\left[1 + \frac{RC}{\tau_\sigma}\right] \tag{19}$$

Subsequently, Eq. (5) underestimates the mobility by a factor $(1 + RC/\tau_\sigma)$. In fact, in the limit $RC \gg \tau_\sigma$, the mobility obtained by Eq. (5) saturates to $\mu_{CELIV} \sim d/enR$, becoming independent of the actual mobility μ of the active layer. In other words, a necessary requirement for Eq. (5) to be valid is that $R \ll d/en\mu$, or equivalently

$$\mu \ll \frac{d}{enR_S S} \tag{20}$$

For typical values of $R_S = 50\ \Omega$, $S = 4$ mm^2 and $d = 100$ nm, this corresponds to $\mu \ll 3 \times 10^{-3}$ cm^2/Vs when $n = 10^{16}$ cm^{-3}. This suggests that the previously reported CELIV mobilities on high-mobility thin-film materials,[29] such as perovskite solar cells, might be limited by the series (load) resistance of the measurement circuit (or the electrode/transport layers).

This is illustrated in Fig. 6, where the extracted CELIV mobility as a function of input mobility, is simulated. Indeed, at large mobilities, corresponding to small τ_σ (note that $qn\mu = \varepsilon\varepsilon_0/\tau_\sigma$), a saturation of the mobility extracted using Eq. (5) is obtained, resulting in an underestimation of the

mobility by several orders of magnitude. Conversely, the RC-induced error in the extracted mobility is drastically reduced by using Eq. (18) instead, as demonstrated in Fig. 6.

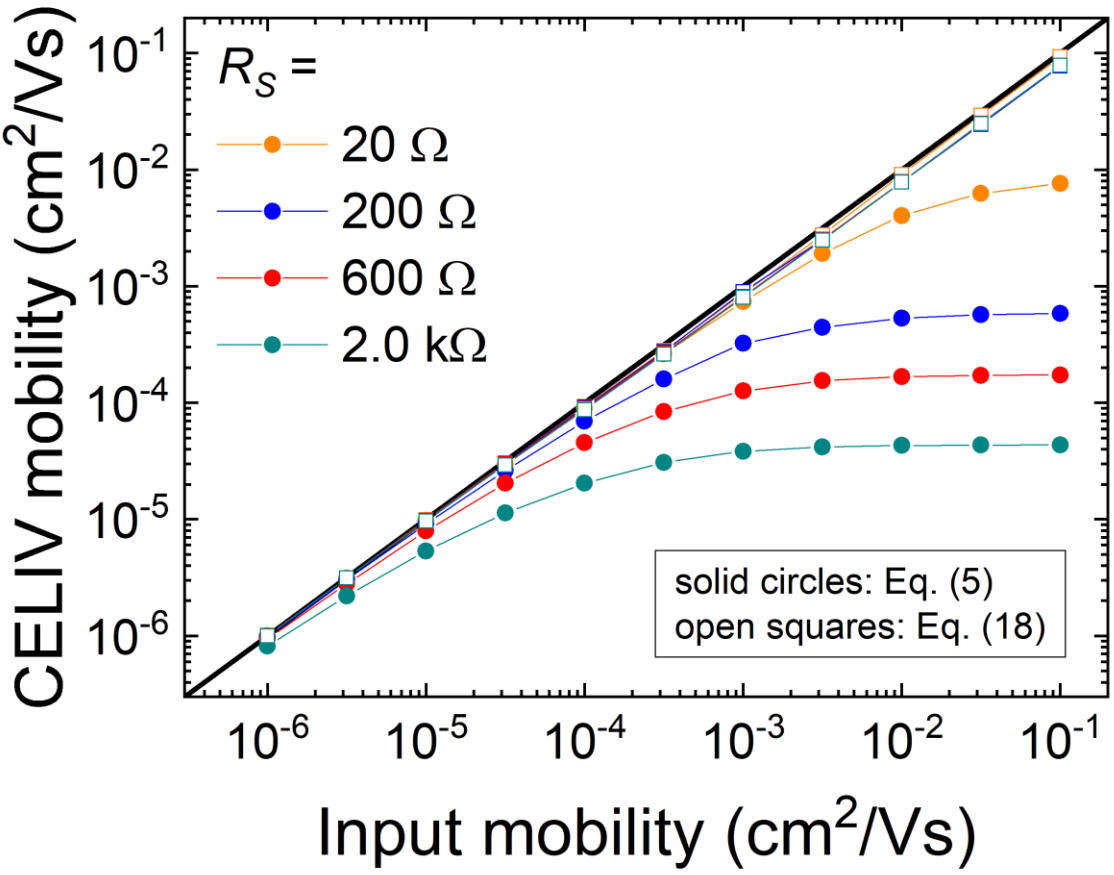

Fig. 6. The extracted CELIV mobility as a function of the input mobility used in the simulations are shown for the different RC (from Fig. 5), assuming a device area of $S = 0.10$ cm^2. The filled circles and open squares correspond to mobilities extracted using Eq. (5) and Eq. (18), respectively. A voltage ramp up rate of 10^5 V/s and a carrier density of 6×10^{15} cm^{-3} ($\Delta j_{max} \sim j_0$) has been assumed, whereas $d = 200$ nm.

3.5. Other effects

The above considerations assume carrier distributions that are uniform at $t = 0$ (when the ramp up voltage pulse is applied). This corresponds to devices with optically thin active layers. In thicker films, the absorption profile needs to be taken into account in the mobility determination: $\mu = 2K_\alpha^2 d^2/3At_{max}^2$, where K_α is the correction due to the non-uniform carrier profile. The effect of the absorption profile has been clarified in earlier reports.[30] In the limit when all carriers are generated as thin sheet at the surface (surface photo-generation) it can be shown that $K_\alpha \to \sqrt{3}$ for $\Delta j_{max} < j_0$.[2,30] In the intermediate regime, however, K_α takes a value between $K_\alpha = 1$ (uniform carrier profile) and $K_\alpha = \sqrt{3}$ (surface photo-generation), with the mobility thus varying within a factor-of-three. It should be noted, however, that depending on the delay time between the charge generation pulse and the charge extraction pulse, photo-induced carriers usually have some time to diffuse and redistribute, leading to a more uniform carrier distribution once the ramp up rate is applied. This is particularly true when the device is initially held at open-circuit conditions, under constant illumination, prior to the extraction pulse.

In this work, we have also neglected the effect of trapping during the charge extraction process. When trapping is significant, an A dependence of the mobility is expected. For shallow traps, the mobility obtained in the limit of large A is given by the mobility of the free carriers, whereas the mobility extracted with lower A reflects an effective trap-controlled mobility.[1] However, in case of broad trap distributions, the charge transport is expected to become highly dispersive; under these conditions, the associated time dependence of the mobility needs to be taken into account.[31]

It should be stressed, however, that in general many different effects might be occurring at the same time, influencing the mobility determination in CELIV in different ways. In order to account for

these effects and accurately determine the device mobility, numerical device simulations are needed, preferably performed in combination with several different experimental techniques.[32]

4. Conclusions

In conclusion, we have shown by means of drift-diffusion simulations that the standard equations used for the mobility determination in photo-CELIV underestimates the mobility at moderate conductivities under conditions when both carrier types are mobile in the device. The error in the mobility determination is largest in case of balanced mobilities, increasing with increasing $\Delta j_{max}/j_0$ and decreasing voltage ramp up rates. In case of different mobilities the extracted mobility is composed of a combination of the electron and hole mobility, dominated by the faster carrier mobility. Moreover, we also show that simply introducing a blocking layer is by itself not sufficient to suppress the extraction current transient for one type of carriers in photo-CELIV. Whereas the influence of two mobile carrier give rise to an underestimation of the mobility, the effect of bimolecular recombination taking place during the extraction pulse generally leads to an overestimation of the mobility.

Finally, also the effect of the series resistance of the external circuit is clarified. The associated RC time constant delays the time of the current maximum, leading to an underestimation of the mobility with Eq. (5). Apart from the relation between t_{max} and the RC time constant, the underestimation is also dependent on the ratio between RC time constant and the dielectric relaxation time of the photo-induced carriers. In thin-film devices with relatively large mobilities and high carrier concentrations, the mobility in CELIV might be underestimated by several orders of magnitude if the series resistance is not taken into account.

Acknowledgements

Helpful discussions with Professor Ronald Österbacka are acknowledged. Partial financial support from the Academy of Finland through Project No. 279055 and Jane and Aatos Erkko foundation is acknowledged. O. J. S. acknowledges funding from the Swedish Cultural Foundation in Finland.

References

[1] G. Juška, K. Arlauskas, M. Viliunas, J. Kocka, *Phys. Rev. Lett.* **84**, 4946 (2000).

[2] A. Pivrikas, N. S. Sariciftci, G. Juška and R. Österbacka, *Prog. Photovolt: Res. Appl.* **15**, 677 (2007).

[3] R. Österbacka, A. Pivrikas, G. Juška, K. Genevičius, K. Arlauskas, H. Stubb, *Current Applied Physics* **4**, 534 (2004).

[4] A. J. Mozer, G. Dennler, N. S. Sariciftci, M. Westerling, A. Pivrikas, R. Österbacka, G. Juška, *Phys. Rev. B* **72**, 035217 (2005).

[5] A. Baumann, J. Lorrmann, D. Rauh, C. Deibel, and V. Dyakonov, *Adv. Mater.* **24**, 4381 (2012).

[6] A. Armin, G. Juška, M. Ullah, M. Velusamy, P. L. Burn, P. Meredith, A. Pivrikas, *Adv. Energy Mater.* **4**, 1300954 (2014).

[7] G. Juška, N. Nekrašas, K. Genevičius, *J. Non-Cryst. Sol.* **358**, 748 (2012).

[8] O. J. Sandberg, M. Nyman, S. Dahlström, S. Sandén, B. Törngren, J.-H. Smått, R. Österbacka, *Appl. Phys. Lett.* **110**, 153504 (2017).

[9] J. Lorrmann, B. H. Badada, O. Inganäs, V. Dyakonov, C. Deibel, *J. Appl. Phys.* **108**, 113705 (2010).

[10] O. J. Sandberg, M. Nyman, and R. Österbacka *Phys. Rev. Appl.* **1**, 024003 (2014).

[11] S. Sandén, O. J. Sandberg, Q. Xu, J.-H. Smått, G. Juška, M. Lindén, R. Österbacka, *Org. Electron.* **15**, 3506 (2014).

[12] Y. Gao, A. Pivrikas, B. Xu, Y. Liu, W. Xu, P. H. M. van Loosdrecht, W. Tian, *Synth. Met.* **203**, 187 (2015).

[13] M. Petrovic, T. Ye, C. Vijila, S. Ramakrishna, *Adv. Energy Mater.* **7**, 1602610 (2017).

[14] M. A. Lampert and P. Mark, *Current Injection in Solids*, (Academic, New York, 1970).

[15] K. C. Kao and W. Hwang, *Electrical Transport in Solids*, (Pergamon Press, Oxford, 1981).

[16] O. J. Sandberg, M. Nyman, R. Österbacka, *Org. Electron.* **15**, 3413 (2014).

[17] S. A. Hawks, B. Y. Finck, B. J. Schwartz, *Phys. Rev. Appl.* **3**, 044014 (2015).

[18] O. J. Sandberg, S. Sandén, A. Sundqvist, J.-H. Smått, R. Österbacka, *Phys. Rev. Lett.* **118**, 076601 (2017).

[19] S. Bange, M. Schubert, and D. Neher, *Phys. Rev. B.* **81**, 035209 (2010).

[20] B. Philippa, C. Vijila, R. D.White, P. Sonar, P. L. Burn, P. Meredith, and A. Pivrikas, *Org. Electron.* **16**, 205 (2015).

[21] N. Nekrašas, K. Genevičius, M. Viliunas, and G. Juška, *Chem. Phys.* **404**, 56 (2012).

[22] W. D. Gill, J. Appl. Phys. 43, 5033 (1972).

[23] H. Bässler, Phys. Status Solidi B 175, 15 (1993).

[24] A. Köhler and H. Bässler, Top. Curr. Chem. 312, 1 (2012).

[25] A. J. Mozer, N. S. Sariciftci, A. Pivrikas, R. Österbacka, G. Juška, L. Brassat, and H. Bässler, Phys. Rev. B 71, 035214 (2005).

[26] Integrating $\frac{dl(t)}{dt} = \frac{\mu A t}{d}$, with $\mu = \mu_0 \exp\left(\gamma\sqrt{At/d}\right)$, yields

$$l(t) = \frac{2d\mu_0}{A\gamma^4}\left[6 + e^{\gamma\sqrt{\frac{At}{d}}}\left(\gamma^3\sqrt{\left(\frac{At}{d}\right)^3} - 3\gamma^2\frac{At}{d} + 6\gamma\sqrt{\frac{At}{d}} - 6\right)\right].$$

[27] M.T. Neukom, N.A. Reinke, and B. Ruhstaller, Solar Energy **85**, 1250–1256 (2011).

[28] The solution of $\left[1 + \frac{RC}{\tau_\sigma}\right]\frac{\partial l(t)}{\partial t} + RC\frac{\partial^2 l(t)}{\partial t^2} = \frac{\mu A t}{d}$, with $l(0) = l'(0) = 0$, is given by

$$l(t) = \frac{\mu A}{2d\left[1+\frac{RC}{\tau_\sigma}\right]}\left[t^2 - \frac{2t}{\left[\frac{1}{RC}+\frac{1}{\tau_\sigma}\right]} + \frac{2\left[1-\exp\left(-\left[\frac{1}{RC}+\frac{1}{\tau_\sigma}\right]t\right)\right]}{\left[\frac{1}{RC}+\frac{1}{\tau_\sigma}\right]^2}\right].$$

By inserting $l(t)$ into Eq. (3), and further into Eq. (16), $j(t)$ can be evaluated. Then, after assuming $t_{max} \gg RC/\left[1 + \frac{RC}{\tau_\sigma}\right]$ and $\exp(t_{max}/RC) \gg 1$ (so that the exponential terms can be omitted), an explicit expression for $\mu(t_{max})$ [Eq. (18)] can be obtained. Note that this approximation breaks down at small $\Delta j_{max}/j_0$ when Δj_{max} becomes overshadowed by the charging current of the electrodes (the second term in Eq. (16)).

[29] J. Peng, Y. Chen, K. Zheng, T. Pullerits, and Z. Liang, Chem. Soc. Rev., 2017, 46, 5714-5729 (2017).

[30] G. Juška, N. Nekrašas, V. Valentinavičius, P. Meredith, and A. Pivrikas, Phys. Rev. B 84, 155202 (2011).

[31] O. Semeniuk, G. Juška, J.-O. Oelerich, M. Wiemer, S. D. Baranovskii, and A. Reznik, Sci. Rep. 6, 33359 (2016).

[32] M. Neukom, S. Züfle, S. Jenatsch, and B. Ruhstaller, Sci. Technol. Adv. Mater., 19, 291-316 (2018).